

# EFFECTS OF ENGINE TOPOLOGY ON THE LOW-IRRADIANCE PERFORMANCE OF SOLAR GAS TURBINE SYSTEMS: A FIRST ANALYSIS

**Matthew R. Meas<sup>1</sup>, Theodor W. von Backström<sup>2</sup>, and Johan van der Spuy<sup>3</sup>**

Solar Thermal Energy Research Group (STERG), Dept. Mechanical and Mechatronic Engineering, Stellenbosch University,  
Stellenbosch, South Africa;

<sup>1</sup> mmeas@sun.ac.za

<sup>2</sup> tvb@sun.ac.za

<sup>3</sup> sjvds@sun.ac.za

## Abstract

Considering the stringent environmental evaluation criteria for renewable energy technologies, the low-DNI operation of solar gas turbines will need to be studied as the technology develops. This paper presents an analysis of the hourly changes in the net power output and solar energy fraction of two solar gas turbine systems using a C++ program developed for the simulation of an integrated gas turbine and pressurized air solar receiver. The performance of a solar gas turbine system based on a standard gas turbine is compared against that of a system based on a modified engine topology.

The reference case is based on the Solar Upscale Gas Turbine (SOLUGAS) system, which uses the 4.6MWe Solar Mercury 50 gas turbine generator set, and the comparison case is based on a conceptual modification of the same engine in which the rotational speed of the compressor can be altered without changing the speed of the turbine.

The findings show that modifying the engine topology could improve the average solar share of the system by 3.62 percent relative to the unmodified system and could reduce the average fuel mass flow rate by 2.11 percent. The total thermal energy input needed to develop a given electrical power output is on average reduced by 208kW, corresponding to an average thermal efficiency improvement of 1.47 percent relative to the standard system. Practical implications of the results are described, and the potential to further improve the modified topology is discussed.

**Keywords:** Solar gas turbines; off-design performance; solar irradiance; component matching.

## 1. Introduction

The gas turbine is a technologically mature device with several attributes, such as capacity for relatively high conversion efficiencies and low generation costs, that make it advantageous for use in concentrating solar power systems. It is understandable, then, that research on Brayton cycle and combined cycle concentrating solar power systems is largely focused on development of the less mature high-temperature solar receiver technology, with development of the gas turbines themselves mostly involving the conversion of existing engines for CSP application.

As the development of solar gas turbines progresses, the performance of the technology under low DNI conditions will need to be evaluated to establish how the need for hydrocarbon fuel (typically natural gas or biogas) as a supplementary energy source can be reduced. Fuel backup constitutes an operating expense, while the solar resource is freely available, and the combustion products emitted not only harm the environment but, in some cases, can affect the eligibility of a proposed generation facility for access to financial support mechanisms.

Gas turbine theory dictates that changing the thermal energy supplied to a fixed speed turboshaft will cause the operating point on the component characteristic to be displaced from the design point in order to maintain compatibility of flow and power [1], as depicted in Fig. 1. The displacement of the operating point causes reduction of the efficiencies of the gas turbine components as the volume ratio of hot gas passed by the turbine to cooler air passed by turbine is altered. Given the variability of DNI, displacement of the engine operating point will inevitably occur if a limit is applied to the amount of fuel that may be supplied to a fixed-speed solar gas turbine.

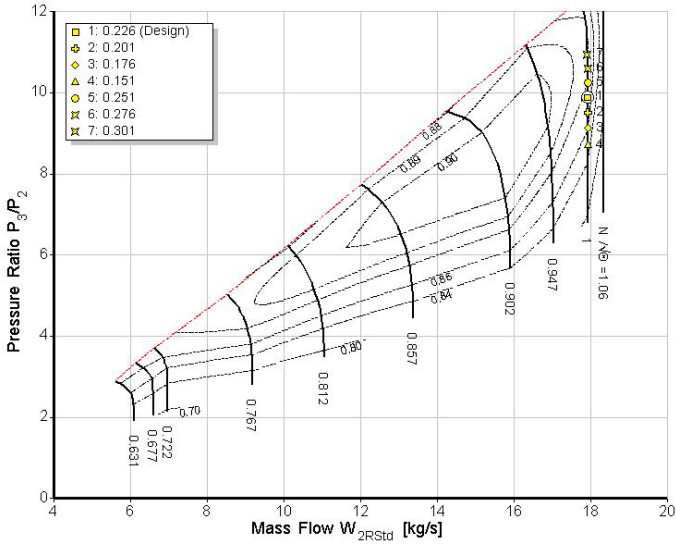


**Fig. 1: Gas turbine compressor characteristic showing operating points at constant rotational speed and different fuel mass flow rates.**

The efficiencies of the gas turbine components can also affect the other components in the flow path. This can be intuited by considering the solar gas turbine system shown in Fig. 2. Reducing in the pressure ratio across the compressor will reduce the temperature of the air supplied to the solar receiver and decrease the fraction of the power developed at the turbine used to drive the compressor. The lower air inlet temperature at the solar receiver should increase the rate at which the solar thermal energy is transferred to the working fluid, which is particularly desirable at lower values of DNI. Improved heat transfer in the receiver should in turn reduce the supplementary energy requirement of the system. Indeed, improving both the collection of available solar energy and the utilisation efficiency of the total thermal energy supplied to the system should result in a lower energy requirement and higher thermal efficiency for a specified net power output.

A closer look at the compressor characteristic in Fig. 1 reveals that displacement of the operating point to a line of lower constant speed would result in a lower pressure ratio, and correspondingly lower compressor air outlet temperature and

power demand. In practice, this would require changing the rotational speed of the compressor while fixing the turbine speed to maintain synchronisation with the frequency of the electric grid.

Configuring a gas turbine so that the compressor and turbine operate at different rotational speeds could prove to be considerably challenging. Yet, the development of a gas turbine with distinct compressor and turbine shaft speeds has been proposed before. Most of these proposals [2, 3] pertain to engines for use in aviation, and the additional weight and complexity a speed altering device would introduce has generally precluded rapid development despite considerable potential in-flight fuel consumption and greenhouse gas emissions.

Rovense [4] has proposed a solar hybrid gas turbine with variable mass flow rate control to address the volume flow rate discrepancies that reduce component efficiencies at lower values of DNI. However, the concept proposed by [4] does not feature different compressor and turbine speeds, instead drawing in more air during periods of higher DNI and relying on operation of the microturbine at pressures above the nominal design pressure.

This work seeks to ascertain whether modifying the engine topology would offer significant improvement in the low-DNI performance of a solar gas turbine, and to get a sense of the feasibility of implementing the necessary modifications. The modelling involved in developing the program used to simulate the operation of the solarised gas turbine system is described, and it is shown how the performance of solar gas turbine based on a commercially available gas turbine compares with that of a system based on an engine in which the compressor is able to operate a rotational speed different to that of the turbine, which is fixed by the frequency of the electric grid.

The results of the simulation show that modifying the engine topology could increase the average solar share by 3.26 percent relative to the unmodified system and could reduce the average fuel mass flow rate by 2.11 percent. The average compressor is found to use 7.6 percent less of the turbine power output compared to the unmodified system, and the associated ratio of the turbine speed to compressor speed is found to range between 1.05:1 and 1.16:1. These findings suggest that the modifications required to leverage the potential improvements in low-DNI performance might not be unjustifiable in cost and complexity. However, inefficiencies in the modification device have not been considered in this work, and require consideration going forward. The findings also suggest potential to improve the low-DNI performance of the modified system further by using a recuperator.

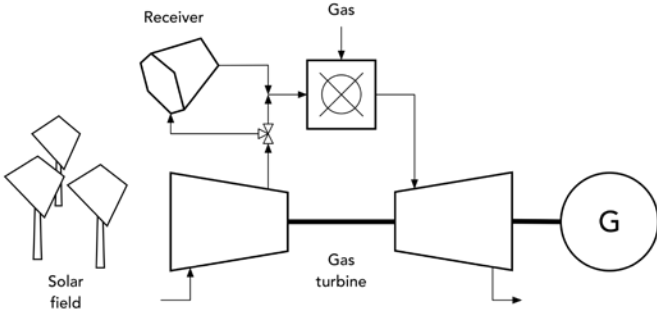


**Fig. 2: Diagram of a solar hybrid gas turbine (SOLUGAS).**

Considering the performance improvement potential shown here for solar hybrid systems, simulation of smaller solar gas turbines should also be undertaken, to assess the possibility of achieving very high solar shares or solar-only operation at lower values of DNI.

## 2. Model description

The solar gas turbine taken as a reference for this work is the Solar Up-scale Gas Turbine (SOLUGAS) system (Fig. 1) commissioned by Abengoa Solar in 2012 [5]. The system, which features a tubular pressurised air receiver and a 4.6MWe Mercury 50 gas turbine unit manufactured by Solar Turbines [6], is the first functioning megawatt-scale system of its kind. Although much solar gas turbines have been developed [European Commission, 2018], moderate power level engines such as the Mercury 50 offer lower spool speeds that are more amenable to alteration and show better potential for lower bulk electricity costs [7].

Given the focus of this work on *low-DNI* performance of solar gas turbines, a relatively low-level model of the heliostat field and solar receiver is developed and applied. Doing so allows the solar thermal energy absorbed through the solar receiver to be determined more accurately than is typically possible using curves fitted to experimental data (assuming such data is available) as it allows the effects of changes in the following salient parameters to be captured:

- Position of the sun relative to the heliostats and central receiver
- Distribution of the concentrated solar irradiance on the components inside the receiver cavity
- Mass flow rate, temperature, and pressure of the air at the receiver inlet
- Heat transfer between the components in the receiver cavity and heat losses to the environment

The development and integration of the component models is described in greater detail below.

### 2.1. Heliostat field

A ray-tracing software (Tonatiuh) is used to obtain the flux distribution on the receiver components at hourly intervals as the DNI and sun position change throughout the day. The simulation is performed using DNI data for the Mariendahl experimental farm in Stellenbosch, with the heliostat field positioned south of the receiver.

While the dimensions of the heliostats used at the SOLUGAS facility in Almería are published in the literature [8, 9], the relative coordinates required to replicate the field layout in the ray-tracing environment are not available.

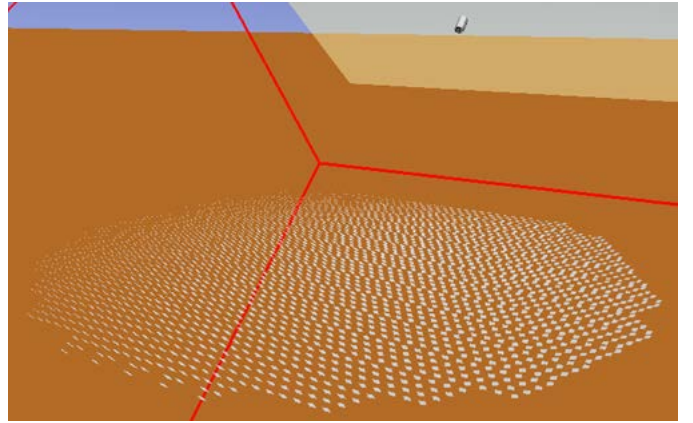


**Fig. 3: The heliostat field and central receiver depicted in the ray-tracing environment.**

As the development of an optimised heliostat field layout is beyond the scope of this work, a densely-packed circular field layout [9] is used (Fig. 4). The heliostat used is the HelioPod, a small-facet heliostat technology developed by the Solar Thermal Energy Research Group (STERG) at Stellenbosch University through an initiative funded by the Technology Innovation Agency (TIA).

Due to the excellent optical performance of the HelioPod, the layout can be used to simulate the performance of a typical heliostat field without having to generate an optimised field layout. Sizing of the field is achieved by adapting the field radius until the requisite optical design power at the target is attained for solar noon, spring equinox. Some of the specifications of the heliostat field model are shown in Table 1 below, with the optical properties of the receiver materials listed with the thermal properties in the following section.

Specification	value	unit
Optical design power	~ 4.6	MW <sub>opt</sub>
Field radius	83	m
Facet optical aperture	1.830 x 1.200	m
Target height	65	m
Target inclination	45	degrees

**Table 1: Heliostat field model specifications.**

### 2.2. Solar receiver

The SOLUGAS receiver, shown in Fig. 4, comprises 10 tube-banks each containing 17 6m-long 19.6mm-bore absorber tubes attached in a staggered formation to a distributor and collector at either end. The tube banks form the walls of the decagonal receiver cavity, which has an aperture diameter of 2.765m, and are lined internally with ceramic fibre insulation.

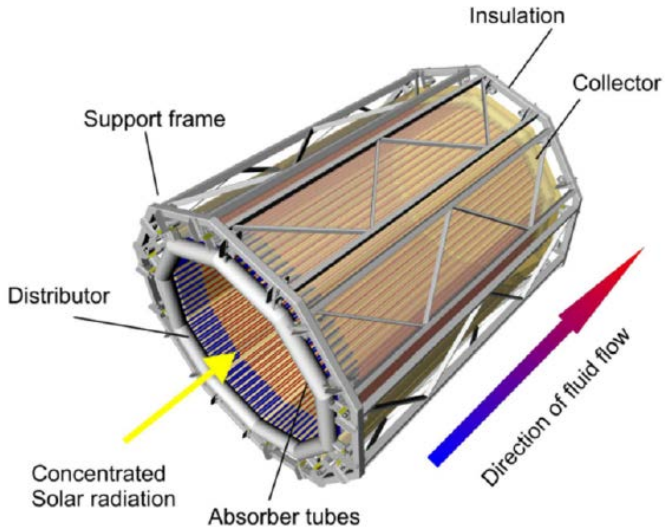


**Fig. 4: Diagram of the SOLUGAS receiver [8].**

The tubes themselves are made of a nickel-based alloy (Inconel® 617) and have an irradiated length of about 5m. A bypass at the compressor outlet (Fig. 1) routes about two thirds of the nominal compressor mass flow rate (approx. 4.5 kg/s) to the receiver, where it is heated up to 800°C. The hot air is then merged with the bypass airstream and the mixture enters the combustor with a temperature below 650°C.

The receiver model developed in the present work applies the finite volume method calculate the thermal energy taken up by the air flowing through the tubes. Critical dimensions for the receiver components are published in the literature [5, 8, 9]. Where necessary, estimates are made for the minor dimensions of the components. The main specifications used in the model are listed in Table 2 below. The model currently assumes constant thermal conductivities, and temperature-dependence will be incorporated at a later stage.

In the discretisation of the energy equation, the conductive heat transfer along the tube and wall surfaces, and the convective heat losses from the surfaces to the environment, are modelled using Fourier's law of heat conduction and Newton's law of cooling. Central differencing is applied, and the edges of the surfaces are modelled as zero-flux boundaries.

Specification	Tube	Wall	Insulation
Thickness [m]	0.001	0.001	0.1
Thermal conductivity [W/Mk]	25	25	0.061
Emissivity	0.88	0.02	-
Reflectivity (diffuse)	0.1	-	0.98

**Table 2: Material properties of the solar receiver components.**

The solar flux incident on each surface is treated as a point source. Forced convection inside the tubes depends both on the temperature of the tube surface and the temperature of the adjacent fluid. It is therefore calculated in a separate step and appended to the source term in the discretised energy equation. Due to the quartic temperature terms in the governing equation, the radiative heat transfer between the surfaces inside the cavity, and radiative heat loss to the environment via the receiver aperture are likewise calculated in a separate step and added to the source-term. The radiative heat transfer is computed using the net radiation method for enclosures, using a virtual surface to account for the open aperture as described by [10]. The view factors used in the radiative heat transfer calculations are computed using the S2S model in ANSYS FLUENT.

Integration between the different steps of the receiver heat transfer model is achieved by calculating the radiative heat transfer and internal forced convection for some at the current timestep using the surface temperatures from the preceding (or initial) timestep. The radiation and internal convection heat transfer values are then used to solve the energy equation and obtain updated values for the surface temperatures, and the process is repeated until surface temperature distribution and the receiver outlet temperature converge. A detailed description of the solution procedure is given by [11].

The receiver geometry is discretised as shown in Table 2. An increase in the number of lateral and longitudinal divisions of the wall, and axial divisions of the tube, showed no appreciable change in the receiver outlet temperature, although a rigorous grid-independence study is still to be undertaken.

Tube axial divisions	20
Tube circumferential divisions	4
Wall longitudinal divisions	20
Wall lateral divisions	20
End surfaces (including aperture)	20 x 20 square grid

**Table 3: Discretisation of the receiver geometry.**

### 2.3. Combustor

The combustor of the Mercury 50 gas turbine is designed to admit air from the cold side of a recuperator. This facilitates replacement of the recuperator with a solar receiver with minimal modification required (Fig. 5) – an attribute which contributed to the selection of the engine for use in the power block of the SOLUGAS system. The combustor is designed to operate using natural gas, for which a lower heating value of 52.6 MJ/kg is calculated and used in this work.

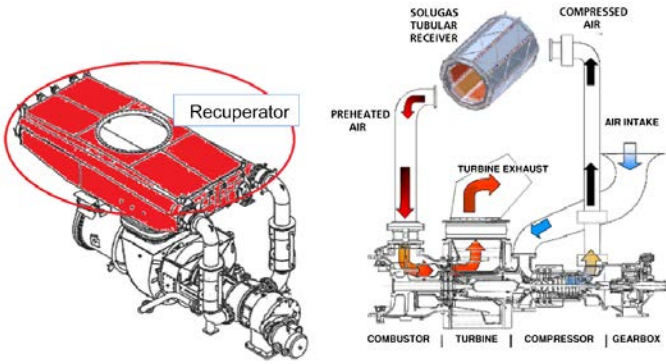


**Fig. 5: Mercury 50 generator set configuration with recuperator (left) and solar receiver (right) [8].**

An energy balance over the combustor gives rise to the expanded equation shown below, with which the combustor outlet temperature can be calculated given the fuel-air ratio  $f$ , and vice versa. In the present work, the fuel air ratio first fixed at an arbitrary value and the operation of the system simulated to get an indication of the corresponding solar energy absorption rate. The fuel mass flow rate is then updated, and the simulations repeated until the desired net power output is achieved.

$$(1 + f)c_{p,comb,out}(T_{comb,out} - 298) + f LHV + c_{p,comb,in}(298 - T_{comb,in}) + f c_{p,fuel}(298 - T_{fuel}) = 0$$

A constant combustor pressure ratio of 1.05 is assumed in the model. This is to be changed at a later stage to account for the effects of changing mass flow rate through the combustor.

#### 2.4. Gas turbine and generator

The theory underpinning the simulation of gas turbine operation is well-developed. Typically, the most challenging aspect is obtaining accurate component characteristic maps for the engine to be simulated, as these are typically not available in the public domain.

The software package GasTurb [12] allows a set of approximate characteristic maps to be generated for a given compressor or turbine by scaling characteristic maps for a similar component, which the user can provide or choose from a selection that the developers have compiled from the literature. The scaling procedure requires that the user know the design point of the component for which the maps are to be generated. The characteristic map taken from the GasTurb library can then be scaled so that a specially-defined scaling point on the map coincides with the design point specified by the user. The feature is used in the present work to generate approximate characteristic maps for the Mercury 50, using the design point specifications listed in Table 2 below.

Specification	value	unit
Rated power	4 600	kW <sub>e</sub>
Compressor pressure ratio	9.9	-
Inlet airflow	17.9	kg/s
Combustor inlet temperature	621	°C
Nominal shaft speed	14 179	rpm
Turbine inlet temperature	1163	°C
Turbine exhaust temperature	365	°C

**Table 2. Solar Mercury 50 specifications [6, 13].**

Of the characteristic maps contained in the GasTurb Map Scaling Library, the characteristic maps for the 15-stage axial 12:1 pressure ratio compressor of a 6MW Ruston gas turbine, and for the *Clean LPT* 3-stage turbine were found to be the closest in specification to the 10-stage axial compressor and 2-stage reaction turbine of the Mercury 50, and were selected for use in the GasTurb map scaling procedure.

GasTurb outputs the characteristic map data in text files, allowing the user to perform calculations with the data using their preferred tool or environment. The map data are formatted as lists of corrected mass flow rate, pressure ratio and efficiency values, arranged according to their corresponding *beta points* – which are predefined *auxiliary coordinates*, along a line of constant speed. The auxiliary coordinates have no physical meaning and are used simply as a means of condensing the data into regular discrete points that can be easily manipulated, for example: to obtain the value of a variable anywhere on the characteristic map by interpolating between neighbouring beta points.

An illustration of compressor map plotted using data obtained from GasTurb is shown in Fig. 6. In this instance, the map is described using 10 beta points on each speed-line, though this can be adjusted in the software. The code written to perform the cycle calculations in this work uses linear splines to interpolate between beta points and determine any third characteristic if corresponding values are known for two others.

The generator is treated as an ideal dynamometer, capable of absorbing any excess power on the shaft. This is considered a reasonable first approximation for the synchronous generators that are typically used in commercially available gas turbine generator sets. The model does not presently consider the magnitude of the electromagnetic torque or windage losses on the generator rotor.

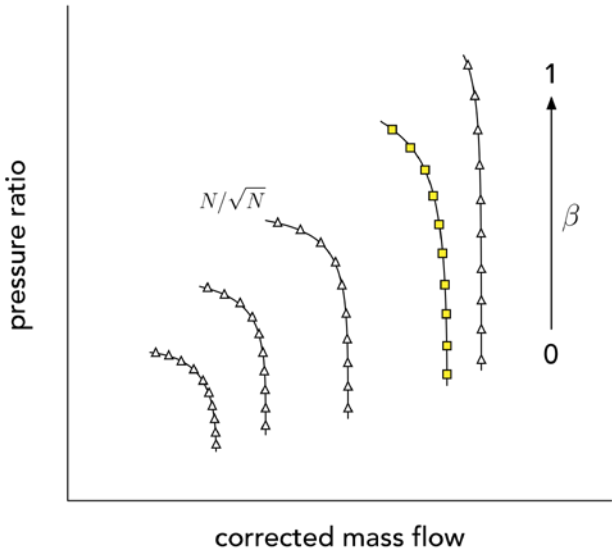


**Fig. 6: A compressor map showing auxiliary points used for interpolation.**

### 3. Simulations

The purpose of the simulation procedure is to determine a feasible operating point for the solar gas turbine system given the time of day (i.e. DNI and sun-position) and fuel mass flow rate. This amounts to locating a pair of corresponding points on the compressor and turbine characteristics for which the compatibility of flow ( $\dot{m}_{turb} - \dot{m}_{comp} = 0$ ) and compatibility of work ( $\tau_{net,shaft} = 0$ ) are satisfied [1].

Two simulations are conducted based on the same procedure, described below. First, the standard, fixed-speed solar gas turbine system (Fig. 1) is simulated. Thereafter, a solar gas turbine system modified to enable operation of the compressor at a rotational speed different to that of the turbine, the speed of which is fixed to maintain synchronisation with the electric grid, as illustrated in Fig 7. The fuel flow mass flow rates are adjusted such that the two configurations produce the same net power output, thus allowing a meaningful comparison between the two systems.

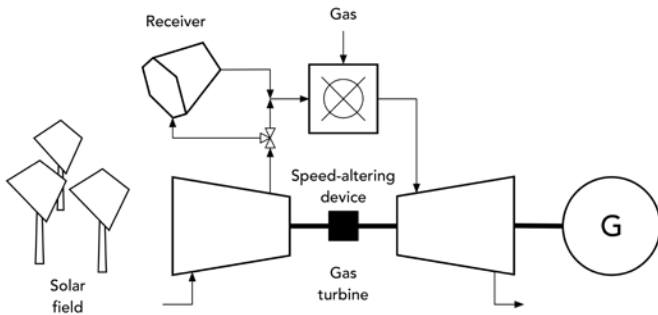


**Fig. 7: The modified solar gas turbine system.**

The difference between the two topologies is most clearly visualised by considering Fig. 6: The potential operating range of the *standard system* is limited to the *line* of square auxiliary points corresponding to the design speed of the engine. By contrast, the potential operating range of the *modified system* spans the entire *envelope* containing both the square and triangular beta points.

The simulation algorithm proceeds as follows for the standard solar gas turbine system:

#### I. Preliminary search:

- i. The compressor mass flow rate, pressure ratio and efficiency are set equal to their values at  $N = 1$  and  $\beta = 0$ .
- ii. The solar thermal energy absorbed in the solar receiver are calculated using the receiver inlet temperature and pressure corresponding to the current compressor operating point and the flux distribution obtained from the ray-tracing simulation.
- iii. The turbine pressure ratio and corrected speed are calculated and used to obtain the corresponding theoretical corrected turbine mass flow rate from the turbine characteristic map.
- iv. The actual turbine corrected mass flow rate is calculated from the compressor mass flow rate and turbine inlet temperature
- v. The flow error (difference between the actual and theoretical corrected turbine mass flow rates) is calculated and stored.
- vi. Increment  $\beta$  and repeat the procedure.

#### II. Fine search:

Starting from the most feasible beta point, apply gradient-based optimisation to locate the operating point in the neighbourhood of the starting point that minimises the flow error.

The procedure for the modified solar gas turbine system differs from the above in that the preliminary search is carried out for the beta points situated on all the other speed-lines on the compressor characteristic map as well, and that the fine search involves optimisation in two dependent variables namely speed and mass flow rate. The simulation algorithm is described in further detail in [14].

### 4. Results

The results of the simulation support the argument that allowing the compressor of the gas turbine to operate at a different rotational speed to the turbine will improve the

compressor efficiency and thus the rate of solar thermal energy absorption in the receiver, whilst reducing the thermal energy required to produce a specified net power output. Indeed, the solar thermal energy absorbed by the modified solar gas turbine system absorbs is between 10 and 47kW higher than that absorbed by the standard system (Fig. 8).

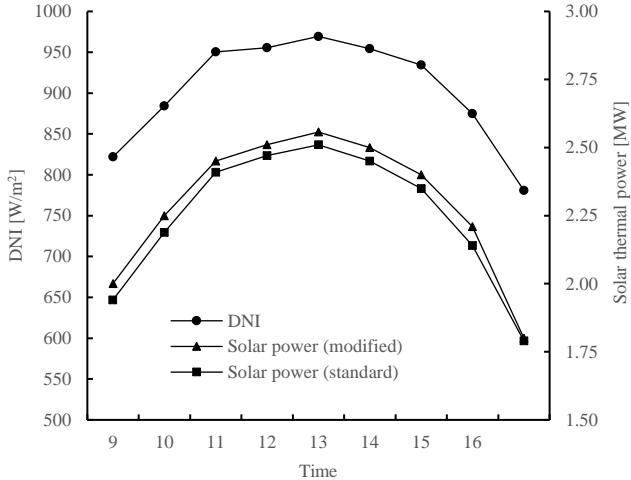


**Fig. 8: Solar thermal power absorbed by the standard and modified gas turbine systems.**

The mass flow rate of fuel necessary to enable the modified system to produce approximately 3.2MW of electric power is also between 6 and 36 g/s (equivalent to 0.307 – 1.86 MJ/s) lower than that needed for the standard system to produce an equivalent amount of power output, as shown in Fig. 9.

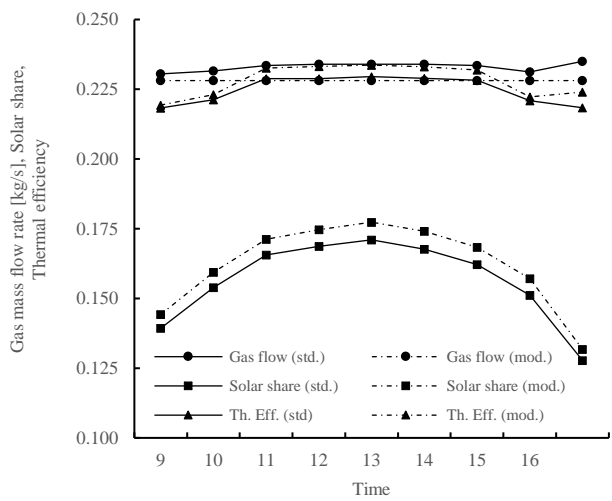


**Fig. 9: Fuel mass flow rate, solar share, and thermal efficiency comparison for the standard and modified gas turbine systems.**

The results of the simulation show good agreement with the experimental data for operation of the SOLUGAS reported by Abengoa. Results from the test campaign in which the receiver

Parameter	value	unit
Electric power output	~ 3	MWe
DNI	900	W/m <sup>2</sup>
Receiver mass flow rate	4.5	kg/s
Receiver inlet temperature	300	°C
Receiver outlet temperature	800	°C
Receiver pressure ratio	~ 8.5	-
Natural gas mass flow rate	~ 0.236	kg/s

**Table 4: Results data from the SOLUGAS system test campaign (800°C receiver outlet temperature) [5].**

was operated with an outlet temperature of 800°C are shown in Table 4 below.

The results of the simulation also confirm that the higher solar share in the case of the modified system can be attributed to two drivers, both of which are related to the improved compressor efficiency (Table 5). The first driver is the lower receiver inlet temperature, which facilitates more effective heat transfer in the solar receiver, and the second is the reduced compressor power demand. Together, these drivers simultaneously increase the solar thermal energy absorbed and the total thermal energy required for a given electric power output in the case of the modified solar gas turbine system. It is worth noting that the turbine outlet temperature calculated for the modified system is quite high. Indeed, recovering the energy contained in this hot exhaust gas by using it to heat the bypass air stream from the compressor outlet might improve the low-DNI performance and reduce the supplementary fuel requirement of the modified system further still.

The ratio of the turbine rotational speed to that of the compressor is found to range from 1.05:1 to 1.16:1. This modest speed ratio and the lower turbine and compressor shaft powers in the modified system suggest that it may be possible use a planetary gearbox with a secondary input torque applied to one of the gears to vary the speed of the compressor. Such a concept was included among the variators considered by [3] in their comparison of continuously variable and fixed ratio transmissions for variable speed helicopter rotors.

The assumptions made for the maximum receiver mass flow rate (admitting at most 4.5 kg/s and rerouting the remaining flow to the combustor) and the electrical power output demanded of the systems (3.2MWe as opposed to the nominal 4.6MWe) might also affect the potential performance improvement attainable by modifying the system. Having obtained good agreement between the simulation results and experimental data for the SOLUGAS system, the refinements

Time	9:00	10:00	11:00	12:00	13:00	14:00	15:00	16:00	17:00
DNI [W/m <sup>2</sup> ]	822.124	884.221	950.357	955.696	969.412	954.296	934.358	874.67	780.875
$P_{out}$ [MW]	3.04	3.147	3.329	3.35	3.369	3.347	3.307	3.128	3.06
<i>Standard system</i>									
$\dot{m}_{air}$ [kg/s]	17.5439	17.5439	17.5439	17.5439	17.5439	17.5439	17.5439	17.5439	17.5439
$\eta_{comp}$	0.862	0.863	0.8648	0.865	0.906	0.865	0.864	0.863	0.862
$P_{comp}$ [MW]	5.31	5.33	5.34	5.34	5.34	5.34	5.34	5.328	5.321
$T_{in,receiver}$ [K]	597.35	597.96	598.625	598.791	598.8713	598.76	598.517	597.83	597.471
$P_{turb}$ [MW]	8.75	8.88	9.02	9.06	9.08	9.05	9.02	8.85	8.773
$\eta_{turb}$	0.867	0.868	0.869	0.8697	0.869	0.864	0.869	0.868	0.8679
$T_{out,turb}$ [K]	772.14	780.447	789.1	791.4534	792.6174	791.0135	787.534	778.84	773.186
<i>Modified system</i>									
$\dot{m}_{air}$ [kg/s]	12.4600	12.597	15.154	15.19	15.209	15.182	15.127	12.57	16.686
$\eta_{comp}$	0.902	0.902	0.9067	0.906	0.906	0.906	0.906	0.902	0.89
$N_{comp}$	0.856	0.858	0.9	0.901	0.901	0.901	0.900	0.858	0.952
$P_{turb}$ [MW]	3.039	3.101	4.076	4.093	4.102	4.089	4.063	3.088	4.757
$T_{in,receiver}$ [K]	538.97	541.19	563.64	564.12	564.37	564.00	563.28	540.72	579.45
$P_{turb}$ [MW]	6.339	6.508	7.723	7.766	7.792	7.756	7.688	6.476	8.169
$\eta_{turb}$	0.857	0.859	0.864	0.864	0.864	0.864	0.863	0.859	0.864
$T_{out,turb}$ [K]	941.34	945.355	847.339	848.226	848.97	847.98	846.38	944.81	782.42

**Table 5: Comparison of results for the standard and modified gas turbine systems.**

to the component models that have been mentioned in the preceding sections will thus be implemented, and a sensitivity analysis undertaken to assess investigate the influence of the relative sizes of the gas turbine and solar receiver.

## 5. Conclusion

The modelling and simulation of two solar gas turbine systems to determine the potential performance improvement attainable through modification of the basic engine topology is described. The results show that allowing the gas turbine compressor to operate at a rotational speed different to that of the turbine, fixed by the frequency of the electric grid, can increase the attainable solar share compared to the standard solar gas turbine configuration in which both the compressor and turbine speed are tied to the grid frequency. The results also indicate that the turbine-compressor speed ratio required to achieve an average increase in the solar share of 3.62 percent is in the range of 1.05:1 and 1.16:1, which could potentially permit modification of an existing gas turbine, or specification of a new system altogether using specially selected components at justifiable cost. Further work is to be undertaken to refine the model to a get a still-clearer indication of the attainable performance improvement.

## References

- [1] Saravanamuttoo, H. I. H., Cohen, H., and Rogers, G. F. C. (2001). *Gas turbine theory*. 5th. New York: Pearson.
- [2] Vratny, P. C., Kaiser, S., Seitz, A., and Donnerhack, S. (2017). Performance Investigation of Cycle-Integrated Parallel Hybrid Turboshafts. *Journal of Engineering for Gas Turbines and Power* 139.
- [3] Misté, G. and Benini, E. (2013). Turboshaft engine performance comparison between CVT and fixed ratio transmission for a variable speed rotor helicopter. *39th European Rotorcraft Forum 2013*.
- [4] Rovense, F., Amelio, M., Scornaienchi, N. M., and Ferraro, V. (2017). Performance analysis of a solar-only gas micro turbine, with mass flow control. *Energy Procedia* 126.
- [5] Quero, M., Korzynietz, R., Ebert, M., Jiménez, A. A., Del Río, A., and Brioso, J. A. (2013). Solugas - Operation experience of the first solar hybrid gas turbine system at MW scale. *Energy Procedia* 49.
- [6] Solar Turbines Inc. (2013). *Mercury 50 Specifications*. Caterpillar Company.
- [7] Schwarzbözl, P., Buck, R., Sugarmen, C., Ring, A., Marcos, M. J. C., Altwegg, P., and Enrile, J. (2006). Solar gas turbine systems: Design, cost and perspectives. *Solar Energy* 80(10).
- [8] Korzynietz, R., Brioso, J. A., Del Río, A., Quero, M., Gallas, M., Uhlig, R., Ebert, M., Buck, R., and Teraji, D. (2016). Solugas - Comprehensive analysis of the solar hybrid Brayton plant. *Solar Energy* 135.
- [9] Lubkoll, M., Hockaday, S. A. C., Harms, T.M., von Backström, T. W., Amsbeck, L., and Buck, R. (2018). Integrating solar process heat into manganese ore pre-heating. *5<sup>th</sup> South African Solar Energy Conference 2018*.
- [10] Modest, M. F. (2003). *Radiative heat transfer*. 2nd. San Diego: Academic Press.
- [11] Hasnaoui, M., Zrikem, Z., Vassseur, P., Bilgen, E. (1990). Solar radiation induced natural convection in enclosures with conducting walls. *Solar & Wind Technology* 7(5).
- [12] GasTurb GmbH (2018). GasTurb 13: Design and off-design performance of gas turbines.
- [13] Lundberg, W. L., Holmes, R. A., King, J. E., Israelson, G. A., Zafred, P. R., Kothmann, R. E., Moekel, M. D., and Veyo, S. E. (2001). A high efficiency PSOFC/ATS – gas turbine power system. Technical report. Siemens Westinghouse.
- [14] Research and Technology Organisation Applied Vehicle Technology Panel. (2002). Performance prediction and simulation of gas turbine engine operation. Technical report. North Atlantic Treaty Organisation.